Abstract In this paper, we will review the state-of-the-art of $LiNbO_3$ based integrated electro-optic modulators and will show how micro-structuring techniques such as etching, domain inversion and thin film processing can be used to realize new configurations which can take the performance to unprecedented levels. In particular, we will review recent results on the use of domain inversion on a micron scale and we report on the fabrication of a chirp-free modulator having ~ 2 V switching voltage and bandwidth of 15 GHz designed by placing the waveguide arms of the Mach-Zehnder interferometer in opposite domain oriented regions. We also review some of the new modulation formats (e.g. DQPSK) that can represent an application development of the presented micro-structured devices. Finally, we address the issue of the integration of the modulator chip in a transmitter board comprising tunable laser, bias-control electronics and RF driver. The requirements of integration can even push further the reduction in size of modulator chips, thus making more crucial the use of micro- and nano-structuring techniques.

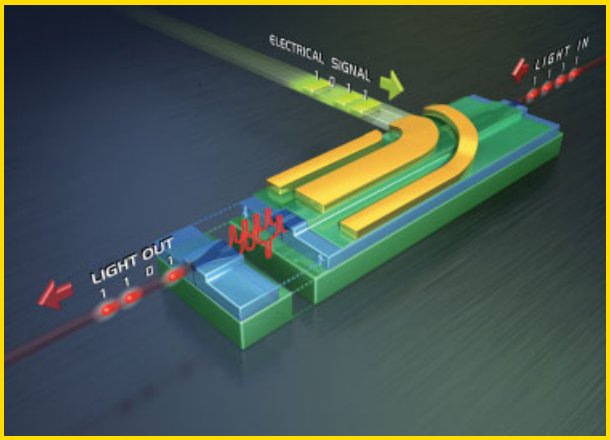

Mach-Zehnder modulator exploiting domain inversion for ultra-low voltage operation.

Micro-structured integrated electro-optic $LiNbO_3$ modulators

Davide Janner[1,*], *Domenico Tulli*[1], *Miguel García-Granda*[1], *Michele Belmonte*[2], *and Valerio Pruneri*[1,3]

[1] ICFO-Institut de Ciencies Fotoniques, Mediterranean Technology Park, 08860 Castelldefels (Barcelona), Spain
[2] Avanex Corporation Sede Secondaria, San Donato Milanese (MI), Italy
[3] ICREA -Institució Catalana de Recerca i Estudis Avançats, 08010, Barcelona, Spain

Received: 25 November 2008, Revised: 19 December 2008, Accepted: 19 December 2008
Published online: 20 January 2009

Key words: Lithium niobate, electro-optic modulators, broad-band modulators, integrated modulators, domain inversion.

PACS: 42.82.Bq, 42.82.Et, 77.84.Dy, 78.30.Hv, 81.40.-z

1. Introduction

Over the past decade the demand for telecommunication services has strongly increased and the consequent requirement for ever larger bandwidth communication system has boomed accordingly. In this scenario, optical networks play a fundamental role as main carriers of information and are continuously growing in importance due to their increasing presence in last-mile connections and fiber-to-the-home (FTTH) links [1]. Inside optical transmission systems, high-speed optical modulators are one of the fundamental building blocks (see Fig. 1 for a typical scheme of an optical link). Among them, external lithium niobate ($LiNbO_3$) modulators are extremely effective [2], in particular for long haul and metro applications, as it is shown by their recent increasing commercial volume. Indeed, total worldwide revenue for digital dense wavelength division multiplexed (DWDM) transmission doubled over last year. This is reflected by the $LiNbO_3$ modulators' market (see Fig. 2) [3]. Note that data refer only to digital communications. These facts are well understood taking into account that $LiNbO_3$ modulation possesses very good performance in terms of extinction ratio, insertion loss, chirp feature and optical transparency – the latter particularly important taking into account the increased use of tunable laser sources. Moreover, with respect to modulators based on semiconductor or

* Corresponding author: e-mail: davide.janner@icfo.es

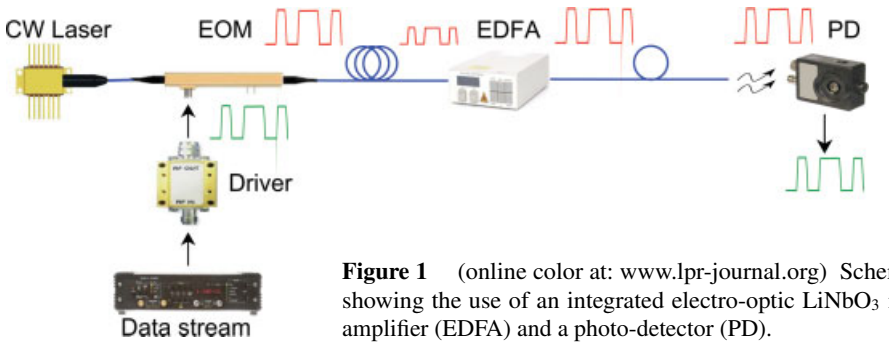

Figure 1 (online color at: www.lpr-journal.org) Schematic of a fiber optic communication link showing the use of an integrated electro-optic $LiNbO_3$ modulator (EOM) an erbium doped fiber amplifier (EDFA) and a photo-detector (PD).

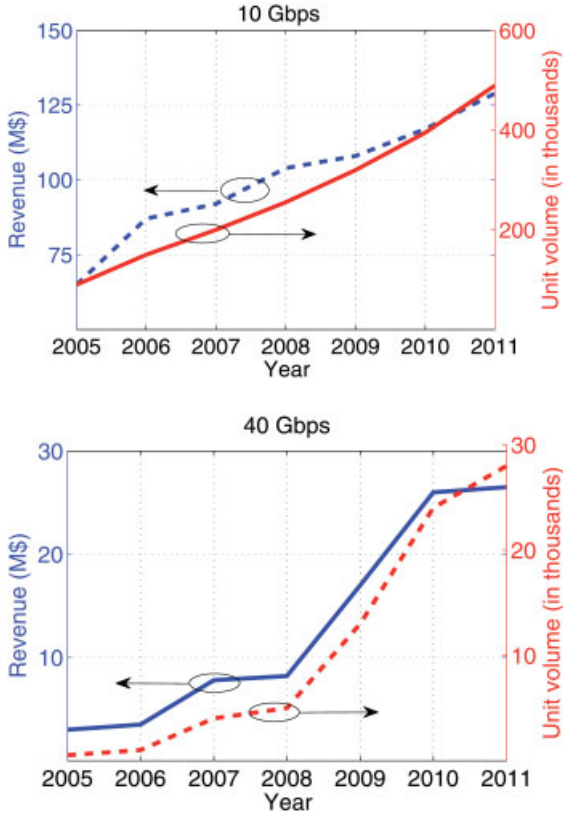

Figure 2 (online color at: www.lpr-journal.org) Trends in $LiNbO_3$ modulators market for digital telecommunications. [3]

other materials, $LiNbO_3$ market share could even become larger if performance, integration and cost further improve. Among others, the required improvements should include at the same time high modulation efficiency (i.e. large modulation bandwidth at low driving voltage) and robust and economic large-scale fabrication process.

Even though the use of velocity matched (VM) traveling wave electrodes configurations [2, 4] greatly increase the modulation bandwidth (BW), the potential of $LiNbO_3$ in terms of modulation efficiency has been far from being fully exploited. In fact, the frequency dependent microwave loss limits the bandwidth of VM modulators: the higher the frequency the higher the microwave loss. Thus, for a given length L, the effective modulation length reduces at higher frequency, so does the efficiency. This makes BW inversely proportional to L, similarly to the switching voltage (V_π) that is needed to obtain a full swing along the modulation curve. Therefore a trade-off exists between V_π and BW and the ratio BW/V_π is used as a figure of merit. To improve the efficiency (increase of BW/V_π), better coupling between the microwave and optical fields is required. Many different solutions [5–23] have been proposed to this end and in Sect. 4 we review some of them focusing our review on modulators' structures that can be fabricated with scalable processes that can be implemented in mass production. In particular, ridge and thin plate modulators can provide a step forward by enhancing the microwave field confinement thus increasing the overall electro-optic interaction.

Besides these approaches that require more additional fabrication steps with respect to standard ones, the exploitation of the polarizability (i. e. domain structure) of $LiNbO_3$ opens interesting scenarios in the micro-engineering of devices toward a higher efficiency. Domain inversion (DI) in ferroelectrics, as $LiNbO_3$, has been widely exploited in all-optical processes, from quasi-phase-matched second harmonic generation to optical parametric oscillation and WDM frequency conversion [24–27]. So far its use in electro-optics, has been mostly limited to quasi-velocity-matching devices using periodic structures [19, 28] or to achieve a desired chirp value for high-frequency and broadband modulators [12]. More recently, domain engineering of z-cut $LiNbO_3$ structures has been proposed to produce large bandwidth and very low voltage modulators where the push-pull effect in the interferometric structure has been obtained by placing the waveguides in opposite-sign electro-optic coefficient regions (i.e. opposite-oriented domains) and under the same electric field [20]. This is in contrast with previous high frequency modulating structures in single domain crystals where the two waveguides are placed under two distinct electrodes having different (usually opposite sign) voltages [2]. With respect to those structures, the proposed DI symmetric scheme allows to achieve at the same time maximum-efficiency, chirp-free and single-drive operation all at once. As an example, we report in this paper on the design, fabrication and test of a DI modulator with 13.5 GHz bandwidth and ~ 2 V switching voltage.

Further increase in efficiency for optical links can be achieved not only by improving the performance of mod-

ulators but also adopting new modulation formats. These type of formats like differential phase shift keying (DPSK) and differential quadrature phase shift keying (DQPSK) improve spectral efficiency (bits/s/Hz) reducing the cost of information transport. Modulators targeted for these novel communication formats can benefit from the micro- structuring techniques and designs reviewed in this paper. Moreover, current trends in advanced applications of optical modulators are also discussed in this review paper, for example we address the integration with lasers, driving and control electronics in a single packaged device.

The paper layout is as follows: in Sect. 2 we will outline some background concepts on integrated electro-optic (EO) modulators, while in Sect. 3, the basic modeling and simulation procedures will be presented. In Sect. 4 we will pay attention to the different structures that can be used in the design of modulators, the performance characteristics attainable with each one, and the fabrication techniques involved. One particular design of ultra low-voltage modulator using DI will be presented. Sect. 5 will introduce the devices for new modulation formats as well as integration possibilities of modulators with tunable lasers and driving electronics. Finally, in Sect. 6 we will draw some conclusions.

2. Mach-Zehnder modulators

To review the key points in modulators design and fabrication we hereafter summarize the main principles and equations of a traveling wave Mach-Zehnder (MZ) $LiNbO_3$ modulator [2,29]. The basic working principle is illustrated in Fig. 3. An input optical field $E = 2$ is equally split between two waveguide branches. In each branch the optical field undergoes a phase shift $\Delta\phi$ which is opposite in phase for the two branches. After the optical signal is recombined it has an electric field $E = e^{j\Delta\phi} + e^{-j\Delta\phi} = 2\cos\Delta\phi$ which results in the optical power modulation curve plotted in Fig. 3. In Fig. 4 we sketch the microwave fields and the cross sections of the basic configurations for a) single drive x-cut modulator, b) single drive z-cut modulator and c) dual drive z-cut modulator. The difference between the z-cut and the x-cut type is the use of optical TM or TE mode respectively for the coupling with the radio-frequency (RF) signal so that the largest EO tensor component (r_{zz}) is always exploited. The difference between the single and dual drive configuration is the possibility of driving with different voltages (V_1 and V_2) the two arms of the Mach-Zehnder. For these modulators the traveling microwave voltage along each arm, apart from an initial phase term, can be written as

$$V(z) = V_0 e^{-\alpha(f_m)z}\sin(k_m\delta z)\,, \qquad (1)$$

where V_0 is the amplitude of the wave, $k_m = 2\pi n_m/\lambda_m$, is the microwave wave-number, $\delta = 1 - n_{opt}/n_m$ is the relative mismatch between the index of refraction of the microwave (n_m) and optical (n_{opt}) waves, f_m is the microwave frequency corresponding to the wavenumber k_m.

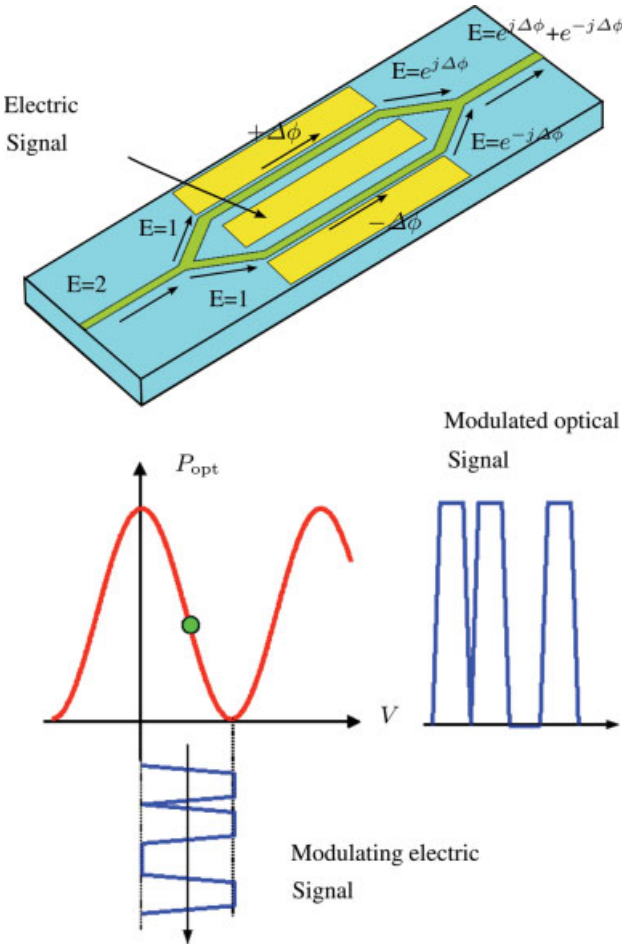

Figure 3 (online color at: www.lpr-journal.org) Modulator schematics and electrical-to-optical transfer curve.

Realistically, we included in Eq. (1) the microwave losses α occurring during propagation and that are related to frequency as $\alpha(f) = \alpha_0\sqrt{f}$ (see [30]) and which can be estimated using finite element method (FEM) (see Sect. 3).

Driven by the microwave, the phase change experienced by the optical wave at the end of the modulator can be written as

$$\Delta\phi(f_m) = -\frac{2\pi}{\lambda}\frac{n_{opt}^3}{2} r \frac{\Gamma}{G}\int_0^L p(z)V_0\sin(k_m\delta z)dz\,, \quad (2)$$

where L is the length of the arms of the modulator itself, λ is the optical wavelength, r is the electro-optic coefficient (in our case for z-cut $LiNbO_3$, $r = r_{zz}$), G is the spatial gap between the two electrodes and Γ is the overlap integral between the optical and microwave electric fields defined as [4]

$$\Gamma = \frac{G}{V_0}\frac{\int E_m\cdot|E_{opt}|^2 dS}{\int|E_{opt}|^2 dS}\,, \qquad (3)$$

with E_m and E_{opt} representing the microwave and optical fields and the integration domain in the modulator cross-

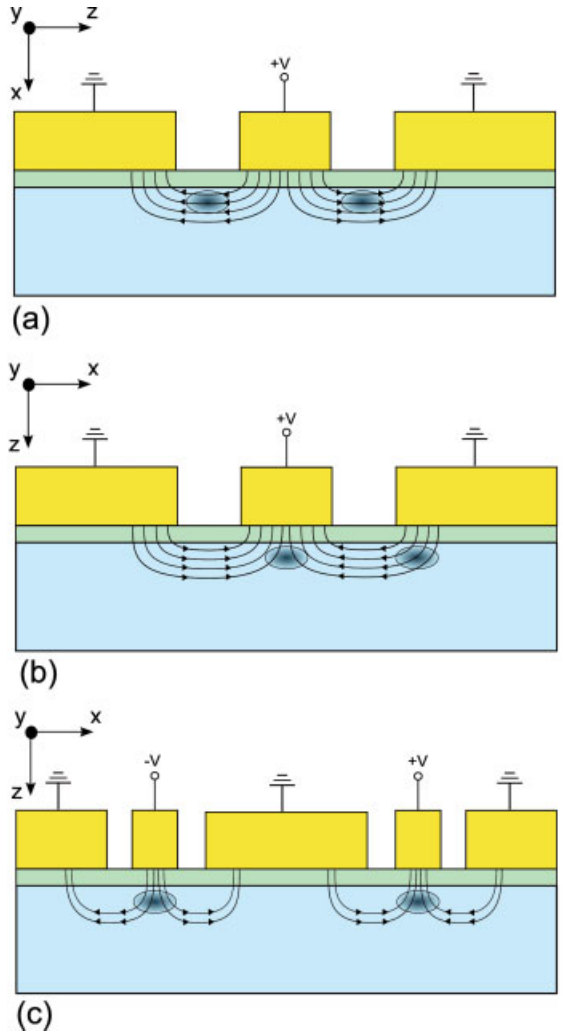

Figure 4 (online color at: www.lpr-journal.org) Cross sections of conventional Mach-Zendher modulators: a) x-cut single drive, b) z-cut single drive, c) z-cut dual drive.

section. The function $p(z) = \pm 1$ in Eq. (2) accounts for changes in the EO response along the modulator due to changes in the EO response of $LiNbO_3$, as in the case of domain inversion. In Fig. 4a we plot for reference the optical and RF field in a classical MZ modulator. Now starting from Eq. (2), the *electro-optic response* for a classic single-drive single domain (unpoled) z-cut modulator, having $p(x) = 1$ everywhere as in Fig. 3a, can be defined as the normalized quantity

$$m(f) = \left|\frac{\Delta\phi(f)}{\Delta\phi(0)}\right| = e^{-\frac{\alpha L}{2}} \sqrt{\frac{\sinh^2\left(\frac{\alpha L}{2}\right) + \sin^2\left(\frac{\xi L}{2}\right)}{\left(\frac{\alpha L}{2}\right)^2 + \left(\frac{\xi L}{2}\right)^2}} \tag{4}$$

with $\xi = 2\pi f_{\mathrm{m}}(n_{\mathrm{m}} - n_{\mathrm{opt}})/c_0$ and c_0 being the speed of light in vacuum. Using Eqs. (2) and (4) we can derive the expression for the switching voltage – corresponding to a phase change of π and producing a theoretical zero optical output – and an estimate of the bandwidth (in GHz) for lossless ($\alpha_0 = 0$) propagation:

$$V_\pi = \frac{\lambda G}{2 n_{\mathrm{opt}}^3 L r \Gamma}, \quad BW_{\alpha=0} = \frac{0.181}{\pi(n_{\mathrm{m}} - n_{\mathrm{opt}})L}. \tag{5}$$

This expression clearly shows the inverse dependence on the length of the modulator for BW and V_π. In the case of dual-drive modulators [2], any asymmetry or deviation in the electrodes or waveguide geometry leads to unbalance in the modulator response, thus introducing a chirp in the modulated signal. This effect is estimated by the chirp parameter η defined as:

$$\eta = \frac{\Gamma_1 - \Gamma_2}{\Gamma_1 + \Gamma_2} \tag{6}$$

where Γ_1 and Γ_2 are the overlap integrals between optic and microwave fields in the first and the second waveguide arms respectively. Especially in long haul transmission, the ideal case is when $\eta = 0$. For this reason, besides bandwidth and switching voltage, the chirp parameter is also considered in the design and fabrication of modulator to be employed in optical links.

In order to increase the efficiency of a modulator the ratio BW/V_π is to be increased. A direct way to obtain this is to increase the overlap integral Γ. To this end, some solutions have been proposed (see Fig. 6). In these geometries the increased overlap is achieved either through a deformation of the modulating field lines (ridge and thin plate) or the placement of the waveguides under a narrower and more efficient electrode (DI inverted push-pull) as we detail in later sessions.

3. Modeling and design

The ideal modulator has large bandwidth, low drive voltage, and a microwave impedance well matched to standard RF drive electronics. However, the fabrication characteristics on which these modulator properties depend often involve trade-offs, e.g. long interaction length limits bandwidth and decreases drive voltage. Modulator design thus entails understanding the design objective and choosing a suitable modulator structure which adequately balances these tradeoffs. Realistically, the large number of structural characteristics impacting modulator performance make it difficult to experimentally sample the entire modulator design parameter space. This difficulty makes computational simulation a natural method for exploring the modulator design space to predict and enhance modulator properties. Due to the nature of the electro-optic interaction, the design of the modulator in the transversal (cross-section) and longitudinal (propagation) direction can be decoupled. At the end the two designs will be put together and the necessary trade-offs will be searched. As underlined in Sect. 2, the fundamental parameters to be determined are the effective

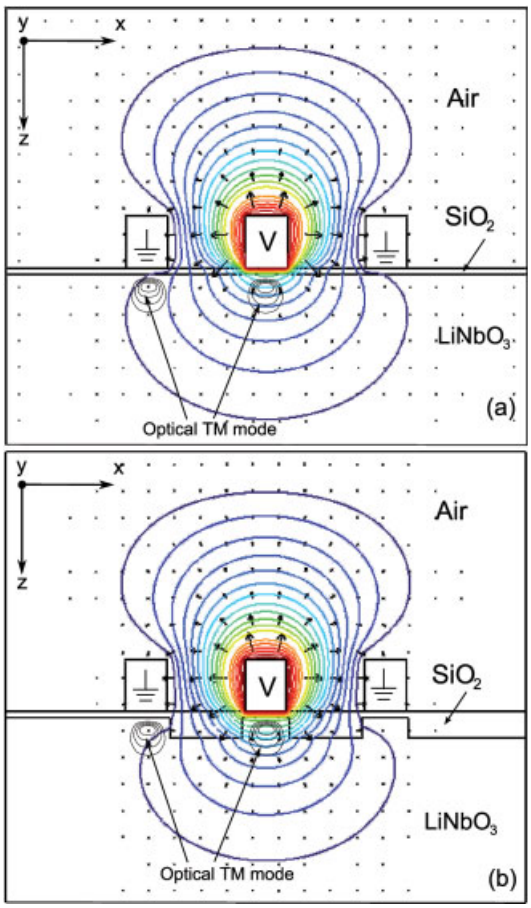

Figure 5 (online color at: www.lpr-journal.org) Comparison of RF field (potential curves in colour) and optical mode of the waveguides (black contour) for a) classical Mach-Zehnder and b) ridge modulator.

microwave index ($n_{\rm m}$) which gives the velocity mismatch (δ) previously defined, electrical loss (α) and the electrical impedance all along the modulator ($Z_{\rm m}$) which is typically matched to 50 Ω to avoid microwave power reflection. To evaluate the microwave frequency dispersion of a coplanar waveguide (CPW) electrode, a full-wave analysis is necessary, and different types of full-wave FEM solvers have been developed [17, 30, 31].

From Maxwell's equations, we can derive the vector wave equation for the microwave field $\mathbf{E}_{\rm m}$ as

$$\nabla \times \nabla \times \mathbf{E}_{\rm m} - k_{\rm m}^2 \underline{\underline{\epsilon}}^{\rm m} \mathbf{E}_{\rm m} = 0 \tag{7}$$

where $k_{\rm m}$ is the free-space wavenumber and $\underline{\underline{\epsilon}}^{\rm m}$ is the diagonal relative permittivity tensor. If we consider a y-propagating microwave as in Fig. 5a, the field can be written:

$$\mathbf{E}_{\rm m}(x, y, z) = \mathbf{E}_{\rm m}(x, z) e^{j\beta_{\rm m} y} \tag{8}$$

and Eq. (7) becomes an eigenvalue problem of the type:

$$[K]\{E_{\rm m}\} = \beta_{\rm m}^2 [M]\{E_{\rm m}\} \tag{9}$$

where the matrices $[K], [M]$ and the discretized RF field $\{E_{\rm m}\}$ follow the definition of Koshiba [31]. In general the propagation constant $\beta_{\rm m}$ is complex and gives two important features of the modulator. Indeed, from β we can derive both $n_{\rm m}$ and α as:

$$n_{\rm m} = \frac{\beta_{\rm m}}{k_{\rm m}}, \quad \alpha = -\,\mathrm{Im}(\beta_{\rm m}) \tag{10}$$

The characteristic impedance of the CPW electrode is calculated using the powerñ-current definition

$$Z_c = \frac{2P}{|I|^2} \tag{11}$$

where P is the modal power, and I is the total y-directional current carried by the center electrode. They are related to the field quantity $\mathbf{E}_{\rm m}$ corresponding to the eigenvector of 7 and the magnetic field $\mathbf{H}_{\rm m}$ calculated from $\mathbf{E}_{\rm m}$ using the following relations:

$$P = \tfrac{1}{2} \iint (\mathbf{E}_{\rm m} \times \mathbf{H}_{\rm m}^*) \cdot \mathbf{n}_y dx dz \tag{12}$$

$$I = \iint \sigma \mathbf{E}_{\rm m} \cdot \mathbf{n}_z dx dz \tag{13}$$

where the integration is done over the entire waveguide cross section for P and over the center electrode for I, σ is the electrode conductivity, $\mathbf{n}_y$ and $\mathbf{n}_z$ are the unit vectors in the y- or z-direction respectively and the asterisk denotes complex conjugation.

The optical field is usually modeled for a fixed polarization (either TE or TM) depending on the type of substrate and/or electrode configuration involved. Thus, the eigenvalue equations for a y-propagating field with a propagation constant $\beta_{\rm opt}$ is written as [32]:

$$\nabla^2 \psi + (n(x, z)^2 k_{\rm opt}^2 - \beta_{\rm opt}^2)\psi = 0 \tag{14}$$

where $\psi = E_x, H_x$ if either TE or TM mode is considered and $n(x, z)$ is the refractive index profile that provides the waveguiding mechanism. Typically the index profile one that comes from titanium indiffusion [33–35].

Once optical and RF fields are computed the overlap integral can be calculated by expression 3 and the corresponding $V_\pi L$ product can be derived from Eq. (5). For comparison, we show in Fig. 5 the computed fields for both RF and optical wave. Note that in the ridge waveguide configuration Fig. 5b, the RF field is much more confined in the waveguide region and the overlap is larger, as it is confirmed by the computed parameters reported in the same figure.

4. Micro-structured integrated modulators

The design methods exposed in Sect. 3 have been employed to explore a wide variety of configurations for Mach-Zehnder modulators. In the following Sect. 4.1 we review

some of the most promising and innovative approaches to enhance modulators performance. In Sect. 4.2 we report on the fabrication techniques that are required by the new generation of modulators and in Sect. 4.3 we show an example of a 10 Gb/s ultra-low-voltage modulator with $V_\pi \sim 2$V fabricated using micro-engineering of domain inversion.

4.1. Device structures

As underlined in Sect. 2, driving voltage and velocity matching are the two most fundamental parameters that define the modulator performance. Both of them are strongly related to waveguide design. In particular, the confinement of light is a fundamental issue if one intends to make the best use of the available electric field. High confinement of optical modes is not easily attainable in diffused waveguides in $LiNbO_3$ due to the gradient index profiles. In contrast, ridge waveguides provide step index contrast in the lateral direction, whereas a diffusion technique is conventionally used to create the confinement in the vertical direction. This allows a stronger lateral confinement which significantly reduces the optical mode size. In a similar way, the ridge structure in a z-cut modulator also provides a better confinement of electrical modulating field within the waveguide region (see Fig. 6a). Therefore, the overlap between optical and modulating fields is optimized with respect to conventional indiffused waveguides. The high confinement also allows reducing the distance between parallel waveguides in a Mach-Zehnder structure, with subsequent enhancement of the push-pull effect.

Another advantage of the ridge waveguides is their ability to decrease the effective refractive index of the modulating microwave. This is possible because part of the $LiNbO_3$ around the waveguide is substituted by a low index medium as air and/or SiO_2, which implies a reduction of the average dielectric constant of the material surrounding the electrodes.

Theoretical studies have been carried out with the aim of finding the best cross-section designs which provide low voltage as well as velocity matching [36, 37]. Calculated results showed that ridge modulators in $LiNbO_3$ are able to reach simultaneous velocity and impedance matching operating in the range of 30 to 40 GHz [17, 30]. The effect of the ridge also implies that electrodes do not need to be so thick as in planar structures (typically in the range of 20 µm) in order to get the matching conditions. The product $V_\pi L$ predicted for these devices was in the order of 8 to 9 Vcm compared to a typical value of 12 Vcm for standard modulators (see Table 1) [36]. Moreover, it was also predicted that the ridge allows smaller bending radius in waveguides without increasing losses, thus improving the integration level of photonic devices [38].

Fabricated ridge structures in MZ modulators have shown bandwidths in the order of 40 GHz with driving voltages as low as 3 V [39, 40]. Also very high bandwidth devices have been made with the use of ridged structures,

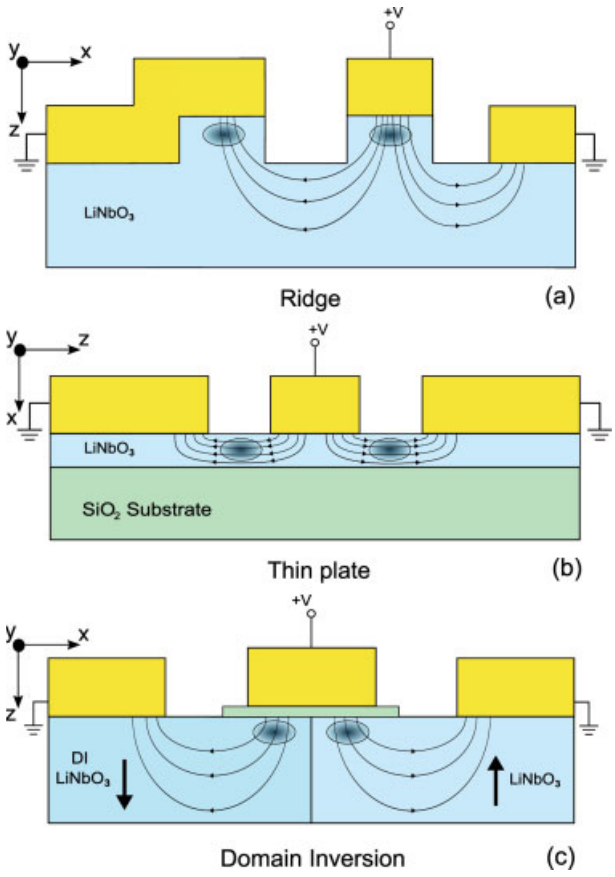

Figure 6 (online color at: www.lpr-journal.org) Comparison between different modulator schemes: a) ridge, b) domain inverted push-pull, c) thin plate.

reaching a bandwidth of 100 GHz with driving voltage in the order of 5 V [41].

Most of the developed ridged modulators were based on a combination of channel diffused waveguides and later selective etching of ridges in the cross section. Nevertheless, it has been recently demonstrated the possibility of creating complete interferometer structures by using high quality ridge waveguides in which the lateral confinement is created only by the ridge walls, and not by a lateral diffusion profile [13].

Apart from ridge modulators, another way of enhancing the field confinement is given by thin plate modulators [7, 42] (see Fig. 6b). For those, the EO crystal is uniformly thinned down to dimensions of the order of 10 µm, by precise lapping and polishing, after an appropriate bonding on a low dielectric constant substrate (e.g. SiO_2), that is used to decrease the effective microwave index. Therefore, the modulating electric field is subjected to a higher confinement and forced to be parallel to the crystal z-axis. Note that, contrary to the ridge and domain inversion geometries in z-cut crystal, the thin plate geometry requires an x-cut crystal. Consequently, the positioning of the optical waveguides with respect to the electrodes changes, so

Structure	$V_\pi \cdot L$ (V· cm)	Γ	Chirp (α)	RF drive
$LiNbO_3$ physical limit	≈ 3.6	1	0	Single
Standard CPW [2]	≈ 12	0.3	$\neq 0$	Single
Dual drive CPW [2]	≈ 8	0.45	arbitrary ($= 0$)	Dual
CPW with longitudinal DI [12]	≈ 12	0.3	≈ 0	Single
Ridge [38, 43]	≈ 8	0.6	≈ 0	Single
Thin plate [7, 42]	≈ 9	0.4	≈ 0	Single
Domain inverted push-pull [20]	≈ 9	0.4	0	Single

Table 1 Comparison of the performances of different configurations.

that the maximum EO tensor component (r_{zz}) is exploited. Waveguide fabrication relies on traditional techniques like Ti-indiffusion and no SiO_2 buffer is needed due to the configuration of electrodes required for x-cut $LiNbO_3$ modulators.

While both ridge and thin plate modulators work on the optical and/or RF field confinement, DI aims at improving the coupling by allowing simpler electrode configurations. For instance, as sketched in Fig. 6c the opposite phase change in the two arms of z-cut modulator can be obtained by DI letting the waveguides being under the same electrode. The advantage of such a configuration consists in the fact that chirp-free operation is guaranteed and a higher overlap integral with respect to classical configuration (see Table 1) can be obtained. Note also that in Fig. 6c there is a silica buffer layer between the hot electrode and the lithium niobate substrate. This layer ensures at the same time low optical loss by keeping the evanescent optical field low in the lossy metal electrodes and velocity matching between the traveling optical and microwave fields.

As it is pointed out in Table 1, with respect to previous structures of CPW modulators driving voltages (for similar device length) are close to those offered by dual drive structures (two waveguides under two hot electrodes driven by opposite sign voltages), with the advantage of being single drive, hence in the absence of any synchronization issue between two different microwave lines. On the other hand the typical single-drive structure in single-domain z-cut has one of the two waveguides under the ground electrode, which induces a lower electro-optic effect due to field spreading compared to the other waveguide under the narrower hot electrode. The result is that the typical driving voltage is about 1.5 times that of a dual-drive structure and 1.4 times that of the proposed geometry. Instead in the DI structure chirp-free operation is a consequence of the symmetry of electrodes with respect to waveguides, so that optical fields traveling in the two Mach-Zehnder arms experience same-amplitude (though opposite in sign) phase shifts. This feature makes the modulator usable in a broad range of applications.

Moreover, pyroelectric effects which are detrimental for thermal stability are reduced by the simultaneous presence of a domain inversion boundary and a symmetric structure (both optically and electrically) . In fact, under temperature variations domain inversion (opposite crystal orientations) causes opposite-sign charges to develop at the interfaces and to produce opposite sign electric fields in the waveguides which tend to cancel each other out, thus reducing thermal drifts. Longitudinal domain inversion can be used to appropriately induce the targeted chirp in single-drive asymmetric structure [12] or to tailor the electro-optic response to embedding optical filtering into the modulator [44].

4.2. Micro-engineering techniques

Etching is a very important process in the fabrication of micro-structured devices in $LiNbO_3$. In particular, it is fundamental in the development of ridge modulators.

Two main kinds of etching techniques can be employed: dry etching and wet etching. Dry etching techniques generally involve the use of a plasma or ion beam to physically (or physically and chemically) remove exposed parts of the material. Focused ion beam etching was reported in the fabrication of waveguides for complex devices [42]. Nevertheless, the use of a lithographic mask together with a large area etching is more suitable for batch production. One of the advantages of these techniques is that they are very controllable and produce highly anisotropic result, which leads to vertical (or slope controlled) etched walls. Plasma etching using fluorine and argon compounds is able to etch $LiNbO_3$ with accuracy, although residual deposits of lithium compounds from the chemical reaction make more difficult to reach very high wall slopes. Therefore, the plasma etching of proton-exchange $LiNbO_3$, which has a reduced lithium concentration, is used to decrease the amount of deposits and obtain vertical etched surfaces [45, 46].

Dry etching techniques produce accurate shaping of the material surface but, generally, a relatively high wall roughness that can produce important optical loss in waveguides. For the use of X-cut ridge waveguides in $LiNbO_3$, plasma etching is currently the best option [47]. Nonetheless, z-cut $LiNbO_3$ can be effectively processed by the wet etching technique [48]. This technique uses HF based compounds in order to selectively etch the -z crystal face. Patterning techniques include the use of Cr metal masks [49], proton-exchange [50], or domain inversion, which allows for control of the wall slope [51]. Even negative slopes have been obtained by combining the wet etching techniques with oxygen implantation [52].

As it was said in Sect. 4.1 a different approach to field confinement is obtained by thinning down the $LiNbO_3$ substrate to thicknesses of few microns. Indeed, in recent years there has been much interest in obtaining single-crystal

thin film $LiNbO_3$ also because it would be useful for enabling integration of $LiNbO_3$ devices on heterogeneous substrates. A number of different techniques have been used to study the deposition of $LiNbO_3$ and other ferroelectric films, such as $BaTiO_3$ and $PbTiO_3$, onto various substrates. Traditionally, thin films are obtained by chemical vapor deposition (CVD) [53], Sol-Gel processing [54], RF sputtering [14], Pulsed-Laser Deposition (PLD) [55] and Ion Implantation [56]. Although high-quality films have been fabricated by these techniques, many of the electrical and electro-optical properties reported are generally not comparable to those for bulk single-crystal material. With respect to other techniques, polishing down the bulk crystal can provide at a time higher quality thin films and an easy implementation in industrial process flow. At a first stage, lithium niobate substrate is bonded to a low dielectric constant material [15, 57] that serves both for decreasing the effective microwave index and for supporting the substrate during thinning. Secondly, it undergoes a first lapping step and is then polished to optical finish. Precision polishing machines and jigs are used to thin the device while the thickness is periodically checked by means of a flat glass plate.

The third micro-engineering technique that we describe is DI. Domain inversion in ferroelectrics is a well known phenomenon according to which the spontaneous polarization of a crystal is reversed at will by locally applying an electric field higher than the coercive field. Several techniques have been studied in recent years to obtain domain inversion in ferroelectric crystals, mainly for nonlinear quasi-phase-matched frequency conversion. These techniques include for example electron-beam poling, [58, 59] electric-field poling, [24–26] and high-voltage atomic force microscope [60]. Among those, electric field poling is a powerful and simple technique usually employed for fabricating periodic domain structures in ferroelectric crystals. It requires very simple facilities and is applicable to many nonlinear optical crystals with the possibility of being easily introduced in mass production.

DI has different implementations even though the basic idea consist in patterning with the desired geometry one face of a $LiNbO_3$ wafer so that the patterned domains to be inverted can come into contact with a conductor – either deposited metal or liquid electrodes – and the other areas are electrically insulated – either by photo-resist or SiO_2 layer. A great number of domain structures have been formed using this technique. However, simple rectangular DI patterns can be employed to enhance modulator performacne as described in Sect. 4.1 (see Fig. 6b). Since the patterning of the poled areas is obtained through photolithographic imprint, it shares the same advantages and limitations. For domain structure such as those in Fig. 6 for instance, the typical area to be poled is hundred microns width and it should be placed between the waveguides with 0.2 µm resolution, features that are well within the feasibility of a standard UV lithographic process.

The experimental setup needed to fabricate this type of device is really simple since it requires only a high voltage generator and some impedances. The electric field is applied all over the patterned surface by liquid electrodes while the patterning is realized by opening a layer of evaporated SiO_2 or photoresist. To show the effectiveness of the technique we report in Fig. 7 a SEM photograph of a DI modulator where domains are revealed by differential etching in HF.

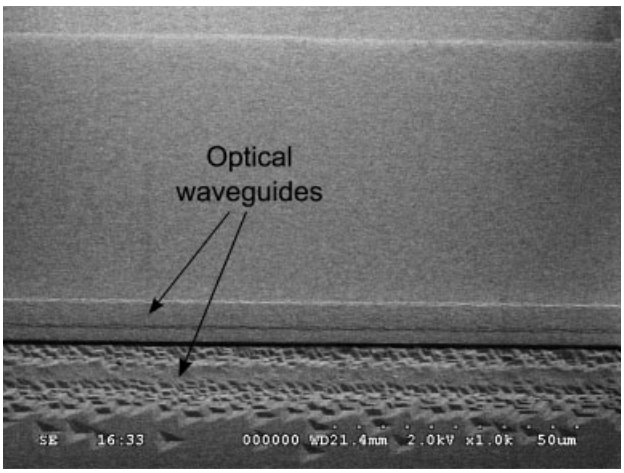

Figure 7 Opposite oriented domains in a DI modulator revealed by differential HF etching. z− domains are etched while z+ remain intact.

4.3. Ultra low-voltage modulator

As an experimental demonstration of one of the modulators reviewed in Sect. 4.1 and the micro-engineering techniques in Sect. 4.2, we report here ona single-drive DI Mach-Zehnder with an active length of $\sim$ 40 mm. The device is designed according to the scheme in Fig. 6c where high-voltage (>10 kV) pulsed poling is performed after Ti indiffusion on the 0.5-mm thick crystal to obtain the cross-sectional inverted domains.

After DI, the modulator chip undergoes standard fabrication, e.g. silica buffer layer deposition, electroplated thick electrode, etc. In Fig. 8 we show the microwave reflection coefficient ($|S11|$) and the corresponding EO frequency response ($|S21|$). From the figure one can see that the electrical reflection is always below −10 dB and the −3 dB EO bandwidth is 13.5 GHz.

The corresponding switching voltage is $\sim$ 2 V (measured at 1 kHz). Therefore the modulator could easily be driven with significant extinction by a low-cost Si-Ge electro-absorption driver which typically provide less than 3 V at 10 Gb/s. In Fig. 9 we report the system measurement setup and the eye diagram obtained form a typical low-voltage modulator employing a Inphi 1015EA driver. The eye opening shows a performance suitable for standard optical communication at 10 Gb/s, including an extinction ratio of 13.65 dB and overall optical losses <2 dB at a wavelength of 1550 nm.

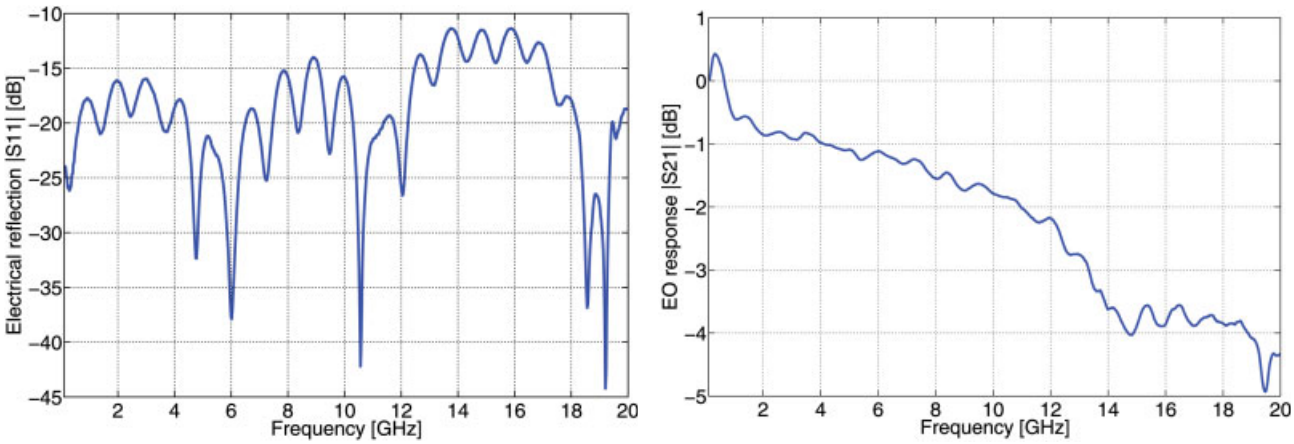

Figure 8 (online color at: www.lpr-journal.org) Domain engineered (as in Fig. 6c) modulator electrical reflection (|S11|) and electro-optic response (|S21|).

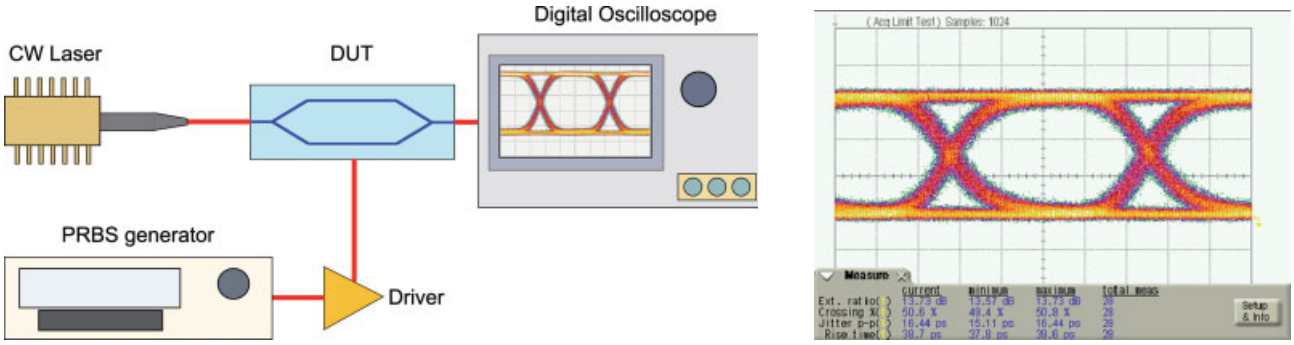

Figure 9 (online color at: www.lpr-journal.org) Test setup (left) and eye diagram measures showing wide opening at 10 Gb/s (right).

5. Advanced applications

5.1. New modulation formats

LN optical intensity modulators are key components in current long-haul WDM high-bit-rate optical communications systems. Nevertheless, novel optical modulators using alternative modulation formats and new architectures are being actively studied in order to match the requirements of next generation systems. On the one hand, these systems will require cost efficiency and adaptability to new environments, such as access networks. On the other hand, a higher capacity over long distance links and core networks will be necessary, primarily due to video applications. Therefore, after years of technology development, the 40 Gb/s is now moving to a generalized deployment phase. Various modulation formats are today employed for 40 Gb/s transmission, with main focus on DPSK and DQPSK, both relying on phase modulation in place of the conventional amplitude modulation.

In the DPSK modulation format the information is phase encoded, with an optical phase switch occurring between different bits. Most often, a Mach-Zehnder modulator is employed, where a modulation over 2 V causes the phase transitions to occur between two neighboring maxima. In this way, the two states exhibit same (full) amplitude, but they show opposite phase. Since modulation occurs over $2V_\pi$, low driving voltage is essential in order to decrease the power consumption of the complete system.

While DPSK is a binary format (i.e. generates one bit per symbol), with DQPSK two symbols per bit are encoded (quaternary format). This allows for considerably better spectral efficiency and brings significant advantage in terms of tolerance to chromatic dispersion and, particularly, to Polarization Mode Dispersion (PMD). To realize the DQPSK modulation, the optical modulator is a key element. This format is generally achieved by employing a nested Mach-Zehnder device, where two MZ modulators are included in a larger interferometer (see scheme in Fig. 10). The inner modulators are to be modulated over $2V_\pi$, but at half rate with respect to DPSK. Reported devices are able to deliver 80 Gb/s DQPSK signals using a double drive signal with an amplitude of 6.5 V [61, 62].

Similar $LiNbO_3$ devices are being studied also to perform simultaneous transmission of baseband and radio sig-

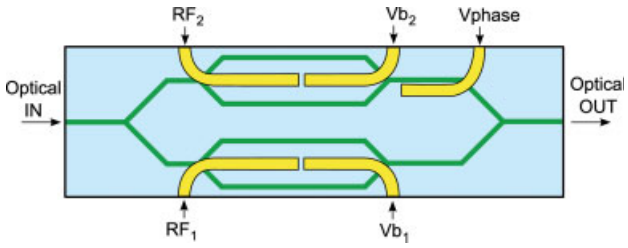

Figure 10 (online color at: www.lpr-journal.org) Scheme of a DQPSK modulator based on a nested MZ with two indipendent RF inputs (RF_1 and RF_2) and bias (Vb_1 and Vb_2). A phase shift is applied by the voltage Vphase to set the working point.

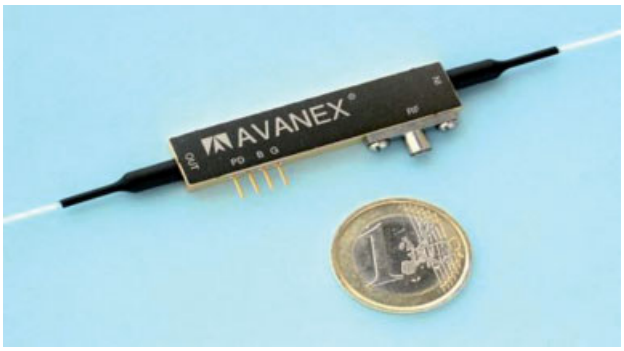

Figure 11 (online color at: www.lpr-journal.org) Example of ultra-small form factor modulator [67].

nals on a single optical wavelength. Due to the fast increase of high data rate demands of wireless and wired networks during the last years, it is desirable to merge both into a single shared infrastructure in order to save costs. One possibility is to modulate and transmit RF and FTTH baseband signals using one external modulator. It has been proposed to use a nested MZ interferometric structure in $LiNbO_3$ for this purpose. In this structure, the RF modulation is implemented in double-side-band carrier-suppressed (DSBCS) amplitude modulation format with a capacity of 622 Mb/s; whereas the baseband signal at 1.25 Gb/s modulated and transmitted using the carrier wave of the same wavelength [63].

Single side-band (SSB) modulation format is also especially useful in optical fiber communication systems. This format requires a narrower operating bandwidth, which makes it adequate for high density wavelength multiplexing. It is also advantageous for long-haul fiber transmission due to less nonlinear optical effects, because of the reduced optical power. One proposed device for this modulation consists of a nested MZ interferometer that works as four parallel phase modulators, driven by signals which are $\pi/2$ shifted [64].

Another approach for SSB modulation employs a single MZ interferometer combined with domain inversion (DI) and a resonant electrode. This modulator has a narrow operating bandwidth because of the resonance effect, with a center frequency of 15 GHz. However, the required modulation power is rather small compared to the traveling-wave modulators and it is useful for radio-over-fiber (ROF) applications [65].

Designs with a three-branch waveguide interferometer have been recently applied to single-sideband carrier- suppressed (SSBCS) modulation and optical frequency shifting operating at a frequency of 15 GHz. Arbitrary control of the phase of optical modulation was also obtained by using the DI engineering. These devices are able to notably contribute to ROF systems and long-haul optical fiber communications due to the optimum use of the transmission bandwidth. Moreover, optical frequency shifting is very attractive in precision laser spectroscopy, quantum optics, and optical measurement systems [66].

5.2. Integration with tunable lasers and electronics

Although reduction in driving voltage can lead to more compact (see Fig. 11) modulators and to an overall cost reduction, packaging costs still account for the majority of device cost. To address this issue there has been in the last years an increasing interest towards integration. The possibility of including several components in the same package also enables more efficient interconnection between the parts and better interoperability.

Lithium niobate modulators lend themselves to integration at several levels. On one hand they need an electrical input driving signal with amplitude of few volts, which is made available by using an RF amplifier. Integrating the driver amplifier with the $LiNbO_3$ modulator brings a number of advantages. First of all, the design of the modulator and of the driver may be optimized for optimal mutual match including e.g. bandwidth optimization and impedance matching. Moreover, the driver design may be optimized so that the output driver voltage is consistent with modulator requirements with the goal of minimizing power consumption. In this respect, lowering the driving voltage brings a substantial advantage. In addition, the electrical interconnections between driver and modulator may be reduced in number (driver can be wire bonded to the lithium niobate device) and optimized in performances with advantages in terms of reduced loss and electrical reflections, and lower cost. For example, by avoiding the use of the conventional RF connectors between driver and modulator, a cost reduction of few tens dollars per device is achieved.

Tunability is also key in today's optical networks. The reason for the interest into tunable wavelengths is twofold. Firstly, tunable sources reduce the inventory as a single part may be employed for any transmission channel as opposed the need for one part number per channel. Secondly, tunable sources pave the way towards reconfigurable networks which allow for extended flexibility in terms of wavelength management and traffic routing, with the eventual advantage of more efficient operation and ultimately reduced operating cost. Also in this respect, lithium nio-

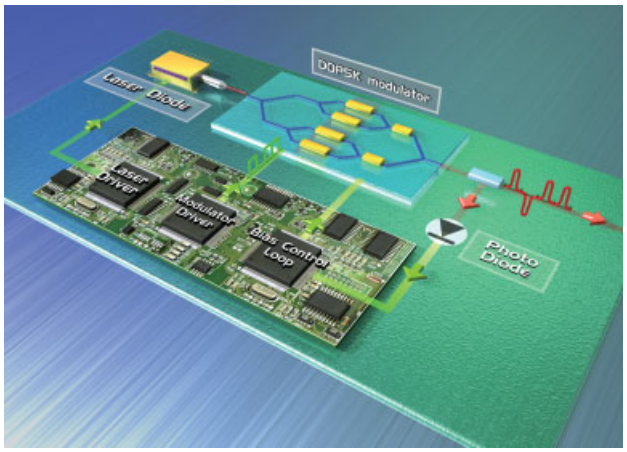

Figure 12 (online color at: www.lpr-journal.org) Scheme of a DQPSK integrated modulator board comprising also laser source, bias control electronics and driver.

bate modulators find their perfect application thanks to the material transparency across C+L band, in contrast to e.g. electroabsorption modulators which generally limit their operating wavelength range to few channels. Integration of tunable laser with lithium niobate modulator is another trend in today's telecom market where integrated tunable laser-modulator assemblies are already commercially available (e.g. JDSU [68]). Besides reducing costs, a key benefit of laser-modulator integration lies in the reduced space occupancy with respect to the discrete approach. This facilitates the development of small form factor linecards and transponders, in line with today's general effort aiming at reducing optical interfaces' dimensions (see Fig. 12).

6. Conclusions

The improvement of performance in lithium niobate modulators can lead to lower cost and higher stability in optical telecommunication links. The performance enhancement goes not only in the direction of an increased bandwidth but also in lowering the driving voltage. As reported in this review, new modulators structures like ridge, thin plate and domain inverted can be effective while their fabrication processes (etching, polishing, bonding and electric field poling) are easily scalable to large mass production. In particular, domain inversion is a simple way to readily obtain a lower switching voltage as demonstrated by the reported example of a modulator having $V_\pi \sim 2$ V and a bandwidth of 13.5 GHz, suitable for inexpensive ultra low-voltage Si-Ge drivers in a 10 Gb/s transmission link.

As a future development, lithium niobate modulators can use micro-structuring to cope also with the challenges of the new modulation formats like DQPSK and SSB that are directed to an increase of spectral efficiency in the modulation which is particularly important when moving to tenths of Gb/s networks.

In the context of telecom market the effort for improving performances needs to be completed by the reduction in packaging costs which account for the majority of the overall modulator price. Recent developments in integration of electronics, driver and laser source pave the way to high integration transceiver and to more efficient and low cost optical networks.

Acknowledgements We acknowledge support from the Spanish national programs Plan Nacional No. TEC2007-60185 and Juan de la Cierva and ICFO-OCE Collaboration program.

Davide Janner received his degree in Physics from Università degli Studi di Milano and his PhD in Physics from Politecnico di Milano, in 2002 and 2006 respectively. He is currently a post-doctoral researcher at the Institute of Photonic Sciences (ICFO) – Spain – carrying out both theoretical and experimental research on the use of domain inversion and etching techniques to obtain highly efficient integrated $LiNbO_3$ modulators and acousto-optic integrated devices. He previously worked in the field of fiber Bragg gratings, photonic crystals, and slow light propagation.

Domenico Tulli received his Master of Telecommunication Engineering from University of Bologna, Italy, in 2006. He is currently a PhD student at the Institut of Photonic Sciences (ICFO) – Spain. His main activity consists in both experimental and theoretical studies of micro- and nano-structured electro-optic crystals using electric-field domain inversion and etching techniques, in particular integrated electro-optic modulators for the telecom industry.

Miguel García-Granda received his degree in Physics in 2003 from the University of Oviedo (Spain). During 2003 he joined the Hanh-Meitner Institut in Berlin (Germany) where he worked in solar cells fabrication and characterization technologies. In 2004 he started his PhD studies between the University of Oviedo (Spain) and the University of Paderborn (Germany) within the topic of ridge waveguide electro-optical modulators. Currently he works at ICFO (Spain) on electro-optical modulation and sensing at microwave and optical frequencies.

Michele Belmonte received his 'Laurea' in Nuclear Engineering *'cum laude'* from the Polytechnic Institute of Milan (Italy) in 1998. He joined Pirelli Componenti Ottici in May 1999 (acquired by Corning Inc. in 2000 and then by Avanex Corp in 2003). At Avanex his current responsibility is for system testing of $LiNbO_3$ modulators and management of tunable laser development. Until 2002 he was responsible for fiber Bragg gratings design within the "FBG" activity. He also carried out experimental research on periodic domain inversion of $LiNbO_3$ for frequency conversion and time resolved spectroscopy. He owns 4 patents in integrated optic technology and published about 25 papers.

Valerio Pruneri received his PhD in Laser Physics/Optoelectronics from the University of Southampton (UK) and his 'Laurea' in Nuclear Engineering from Politecnico di Milano (IT). He is currently an ICREA Professor and group leader at the Institute of Photonic Sciences in Spain. His current applied research interests include micro- and nano-engineered domain inverted electro-optic devices, phononic/photonic crystals for efficient acousto-optics and micro-structured glass fibres (tapered PCF and nanowires) for optical telecommunication, sensing, aerospace and quantum cryptography. Prior to ICFO he had worked for Avanex Corporation, Corning Inc., Pirelli Cables and Systems and the Optoelectronics Research Centre (University of Southampton). He has received more than 25 invitations at major international conferences. He is author or co-author of more than 140 papers, 14 granted patents/patent applications.

References

[1] http://www.fcc.gov/oet/tutorial/ftth tutorial-8-7-03.ppt.

[2] E. L. Wooten, K. M. Kissa, A. Yi-Yan, E. J. Murphy, D. A. Lafaw, P. F. Hallemeier, D. Maack, D. V. Attanasio, D. J. Fritz, G. J. McBrien, and D. E. Bossi, IEEE J. of Select. Topics in Quant. Elec. **6**(1), 69–82 (2000).

[3] Market trends for digital modulators, Tech. rep., Internal survey, 2007.

[4] R. C. Alferness, Microwave Theory and Techniques, IEEE Transactions on **82**(8), 1121–1137 (1982).

[5] A. A. Abou El-Fadl and A. I. Zarea, Modeling and Analysis of $LiNbO_3$ Optical Modulator with Superconducting Electrodes, in: Proceedings of the Canadian Conference on Electrical and Computer Engineering CCECE '06, Ottawa 2006, pp. 846–850.

[6] K. Aoki, J. Kondo, Y. Iwata, A. Hamajima, T. Ejiri, O. Mitomi, and M. Minakata, J. Lightwave Tech. **25**(7), 1805–1810 (2007).

[7] K. Aoki, J. Kondo, A. K. T. Ejiri, T. Mori, Y. Mizuno, M. Imaeda, O. Mitomi, and M. Minakata, J. Lightwave Tech. **24**(5), 2233–2237 (2006).

[8] K. Aoki, J. Kondo, A. Kondo, T. Mori, Y. Mizuno, S. Shimodaira, M. Imaeda, Y. Kozuka, O. Mitomi, and M. Minakata, Phot. Tech. Lett. **16**(12), 2610–2612 (2004).

[9] W. K. Burns, M. M. Howerton, R. P. Moeller, R. W. McElhanon, and A. S. Greenblatt, Broadband reflection travelling-wave $LiNbO_3$ modulator, in: Proceedings of the Technical Digest Optical Fiber Communication Conference and Exhibit OFC '98, San José 1998, pp. 284–285.

[10] W. K. Burns, M. M. Howerton, R. P. Moeller, R. W. McElhanon, and A. S. Greenblatt, Reflection traveling wave $LiNbO_3$ modulator for low V_π operation, in: Proceedings of the IEEE Lasers and Electro-Optics Society Annual Meeting LEOS '97 10th Annual Meeting, San Francisco 1997, Vol. 1, pp. 60–61.

[11] S. J. Chang, C. L. Tsai, Y. B. Lin, J. F. Liu, and W. S. Wang, J. Lightwave Tech. **17**(5), 843–847 (1999).

[12] N. Courjal, H. Porte, J. Hauden, P. Mollier, and N. Grossard, J. Lightwave Tech. **22**(5), 1338–1343 (2004).

[13] M. García-Granda, H. Hu, W. Sohler, and J. Rodriguez-Garcia, Novel structures for broadband electrooptic modulators in $LiNbO_3$, in: European Conference of Integrated Optics, ECIO08, Eindhoven 2008, pp. 79–82.

[14] G. Griffel, S. Ruschin, and N. Croitoru, Appl. Phys. Lett. **54**(15), 1385–1387 (1989).

[15] A. Guarino, G. Poberaj, D. Rezzonico, R. Degl'innocenti, and P. Gunter, Nature Photonics **1**, 487–490 (2007).

[16] H. Haga, M. Izutsu, and T. Sueta, J. Quant Elec. **22**(6), 902–906 (1986).

[17] S. Haxha, B. M. A. Rahman, and R. J. Langley, Optical and Quantum Electronics **36**(14), 1205–1220 (2005).

[18] M. Hochberg, T. Baehr-Jones, G. Wang, J. Huang, P. Sullivan, L. Dalton, and A. Scherer, Opt. Express **15**(13), 8401–8410 (2007).

[19] Y. Lu, M. Xiao, and G. J. Salamo, Appl. Phys. Lett. **78**(8), 1035–1037 (2001).

[20] F. Lucchi, D. Janner, M. Belmonte, S. Balsamo, M. Villa, S. Giurgiola, P. Vergani, and V. Pruneri, Opt. Express **15**(17), 10739–10743 (2007).

[21] K. Noguchi, H. Miyazawa, and O. Mitomi, $LiNbO_3$ high-speed modulator, in: Proceedings of the Pacific Rim Conference on Lasers and Electro-Optics CLEO/Pacific Rim '99, Seul 1999, Vol. 4, pp. 1267–1268.

[22] J. H. Schaffner and R. R. Hayes, J. Lightwave Tech. **12**(3), 503–511 (1994).

[23] J. C. Webster and F. Zernike, Appl. Phys. Lett. **26**(8), 465–467 (1975).

[24] M. Yamada, N. Nada, M. Saitoh, and K. Watanabe, Appl. Phys. Lett. **62**(5), 435–436 (1993).

[25] V. Pruneri, R. Koch, P. G. Kazansky, W. A. Clarkson, P. S. J. Russell, and D. C. Hanna, Opt. Lett. **20**(23), 2375 (1995).

[26] L. E. Myers, R. C. Eckardt, M. M. Fejer, R. L. Byer, W. R. Bosenberg, and J. W. Pierce, J. Opt. Soc. Am. B **12**(11), 2102–2116 (1995).

[27] G. Schreiber, H. Suche, Y. L. Lee, W. Grundkotter, V. Quiring, R. Ricken, and W. Sohler, Appl. Phys. B **73**(5-6), 501–504 (2001).
[28] J. H. Schaffner, US Patent 5278924: Periodic Domain Reversal Electro-Optic Modulator, 1994.
[29] K. W. Hui, K. S. Chiang, B. Wu, and Z. H. Zhang, J. Lightwave Tech. **16**(2), 232–238 (1998).
[30] S. Haxha, B. M. A. Rahman, and K. T. V. Grattan, Appl. Opt. **42**(15), 2674–2682 (2003).
[31] M. Koshiba, Y. Tsuji, and M. Nishio, J. Microwave Theo. Trans. **47**(9), 1627–1633 (1999).
[32] T. Tamir (ed.), Guided-Wave Optoelectronics (Springer-Verlag, 1990).
[33] E. Strake, G. P. Bava, and I. Montrosset, J. Lightwave Tech. **6**(6), 1126–1135 (1988).
[34] W. K. Burns, P. H. Klein, E. J. West, and L. E. Plew, J. Appl. Phys. **50**(10), 6175–6182 (1979).
[35] M. Fukuma, J. Noda, and H. Iwasaki, J. Appl. Phys. **49**(7), 3693–3698 (1978).
[36] O. Mitomi, K. Noguchi, and H. Miyazawa, J. Microwave Theo. Trans. **43**(9), 2203–2207 (1995).
[37] B. M. A. Rahman and S. Haxha, J. Lightwave Tech. **20**(10), 1856–1863 (2002).
[38] N. Anwar, S. S. A. Obayya, S. Haxha, C. Themistos, B. A. Rahman, and K. T. V. Grattan, J. Ligthwave Technol. **20**(5), 854–861 (2002).
[39] W. K. Burns, M. M. Howerton, R. P. Moeller, R. Krahenbuhl, R. W. McElhanon, and A. S. Greenblatt, J. Lightwave Tech. **17**(12), 2551–2555 (1999).
[40] M. M. Howerton, R. P. Moeller, A. S. Greenblatt, and R. Krahenbuhl, Phot. Tech. Lett. **12**(7), 792–794 (2000).
[41] K. Noguchi, O. Mitomi, and H. Miyazawa, J. Lightwave Tech. **16**(4), 615–619 (1998).
[42] P. Rabiei and W. H. Steier, Appl. Phys. Lett. **86**(16), 161115 (2005).
[43] M. García-Granda and H. Hu, Design of Broadband Electrooptical Modulators Using Ti:$LiNbO_3$ Ridge Waveguides, in: 5a Reunion Espanola de Optoelectronica, OPTOEL07, Bilbao 2007, pp. 69–74.
[44] D. Janner, M. Belmonte, and V. Pruneri, J. Lightwave Technol. **25**(9), 2402–2409 (2007).
[45] H. Nagata, N. Mitsugi, K. Shima, M. Tamai, and E. M. Haga, J. Cryst. Growth **187**, 573–576 (1998).
[46] H. Hu, A. P. Milenin, and R. B. wehrspohn, J. Vac. Sci. Technol. A **24**, 1012–1015 (2006).
[47] H. Hu, R. Ricken, and W. Sohler, Etching of lithium niobate: From ridge waveguides to photonic crystal structures, in: European Conference of Integrated Optics ECIO08, Eindhoven 2008, pp. 75–78.
[48] K. Nassau, H. J. Levinstein, and G. M. Loiacono, J. Phys. Chem. Solids **27**, 983–988 (1966).
[49] H. Hu, R. Ricken, W. Sohler, and R. B. Wehrspohn, Phot. Tech. Lett. **19**(6), 417–419 (2007).
[50] T. L. Ting, L. Y. Chen, and W. S. Wang, IEEE Photonics Technol. Lett. **18**, 568–570 (2006).
[51] I. E. Barry, G. W. Ross, P. G. R. Smith, and R. W. Eason, Appl. Phys. Lett. **74**(10), 1487–1488 (1999).
[52] D. M. Gill, D. Jacobson, C. A. White, C. D. W. Jones, Y. Shi, W. J. Minford, and A. Harris, J. Lightwave Tech. **22**(3), 887–894 (2004).
[53] Y. Sakashita and H. Segawa, J. Appl. Phys. **77**(11), 5995–5999 (1995).
[54] J. G. Yoon and K. Kim, Appl. Phys. Lett. **68**(18), 2523–2525 (1996).
[55] S. H. Lee, T. K. Song, T. W. Noh, and J. H. Lee, Appl. Phys. Lett. **67**(1), 43–45 (1995).
[56] M. Levy, J. R. M. Osgood, R. Liu, L. E. Cross, G. S. C. III, A. Kumar, and H. Bakhru, Appl. Phys. Lett. **73**(16), 2293–2295 (1998).
[57] M. M. R. Howlader, T. Suga, and M. J. Kim, Appl. Phys. Lett. **89**(3), 031914 (2006).
[58] M. Yamada and K. Kishima, Electronics Lett. **27**(10), 828–829 (1991).
[59] Y. Glickman, E. Winebrand, A. Arie, and G. Rosenman, Appl. Phys. Lett. **88**(1), 011103 (2006).
[60] G. Rosenman, P. Urenski, A. Agronin, Y. Rosenwaks, and M. Molotskii, Appl. Phys. Lett. **82**(1), 103–105 (2003).
[61] T. Kawanishi, T. Sakamoto, T. Miyazaki, M. Izutsu, K. Higuma, and J. Ichikawa, 80 Gb/s DQPSK modulator, in: Proceedings of the Conference on Optical Fiber Communication and the National Fiber Optic Engineers Conference OFC/NFOEC 2007, Anaheim 2007, pp. 1–3.
[62] M. Doi, N. Hashimoto, T. Hasegawa, T. Tanaka, and K. Tanaka, 40 Gb/s Low-drive-voltage $LiNbO_3$ Optical Modulator for DQPSK Modulation Format, in: Proceedings of the Conference on Optical Fiber Communication and the National Fiber Optic Engineers Conference OFC/NFOEC 2007, Anaheim 2007, pp. 1–3.
[63] C. T. Lin, C. F. Peng, P. C. Peng, J. Chen, W. R. Peng, B. S. Chiou, and S. Chi, Simultaneous modulation and transmission of ftth baseband and radio signals on a single wavelength, in: Proceedings of the Conference on Optical Fiber Communication and the National Fiber Optic Engineers Conference OFC/NFOEC 2007, Anaheim 2007, pp. 1–3.
[64] S. Shimotsu, S. Oikawa, T. Saitou, N. Mitsugi, K. Kubodera, T. Kawanishi, and M. Isutsu, IEEE Photonics Technol. Lett. **13**(4), 364–366 (2001).
[65] H. Murata, D. Nakata, K. Ono, and Y. Okamura, Electrooptic single-sideband modulator using resonant electrodes and polarization-reversed structure, in: Proceedings of the (CLEO) Lasers and Electro-Optics Conference on, Baltimore 2005, Vol. 2, pp. 880–882.
[66] H. Murata, M. Anjiki, and Y. Okamura, Optical Suppressed-Carrier Single Side-Band Modulator-Optical Frequency Shifter Utilizing Three-Branch Waveguide Interferometer and Polarization-Reversed Structure, in: Proceedings of the 36th European Microwave Conference, Manchester 2006, pp. 609–611.
[67] http://www.avanex.com/products/datasheets/transmission/2613_pwrbitxs10-1700-2000.pdf.
[68] http://www.jdsu.com/products/optical-communications/products/tunable-transmission-modules/transponder-tunable-cl-band-10gbs-msa-7100-series.html.